Fluctuations of Cloud, Humidity, and Thermal Structure near the Tropical Tropopause

MURRY SALBY

University of Colorado, Boulder, Colorado

FABRIZIO SASSI AND PATRICK CALLAGHAN

Atmospheric Systems and Analysis, Broomfield, Colorado

WILLIAM READ

NASA Jet Propulsion Laboratory, Pasadena, California

HUGH PUMPHREY

University of Edinburgh, Edinburgh, United Kingdom

(Manuscript received 27 March 2002, in final form 10 April 2003)

ABSTRACT

Thermal and humidity structures near the tropical tropopause are studied using microwave satellite retrievals of water vapor, along with contemporaneous dynamical structure in ECMWF analyses and cold clouds in high-resolution global cloud imagery. Examined during November 1991–February 1992, these fields all vary coherently with the outflow from convective centers—in the upper troposphere as well as in the lowermost stratosphere. The outbreak of deep convection is accompanied by diabatic heating below a level between 250 and 150 mb but by diabatic cooling at higher levels. The reversal from heating to cooling is broadly consistent with cumulus detrainment. Through irreversible mixing, that process serves as a heat source for the environment below the level of neutral buoyancy (LNB) but as a heat sink at higher levels. Calculations, inclusive of entrainment, place the LNB very near the observed reversal from heating to cooling.

The outbreak of convection is also accompanied by humidification below 125 mb but by dehydration at higher levels. The reversal from humidification to dehydration coincides with levels where environmental conditions approach saturation. Those conditions suggest the efficient removal of total water from cumulus updrafts, leaving dessicated air to ventilate to higher levels. Cumulus detrainment then acts to humidify the environment beneath the zone of nearly saturated environmental conditions, while dehydrating it at higher levels. Dry air emerges from the region of the coldest cloud. It then extends into the winter hemisphere, along streamlines that characterize the Hadley circulation.

Coinciding with diabatic cooling are stratospheric convergence and downwelling. These features of stratospheric motion amplify simultaneously with divergence at tropospheric levels, which represents the major outflow from deep convection. The deepest convection, found over the equatorial Pacific, coincides with the highest moist static energy. The latter yields an LNB that is some 3 km higher over the equatorial Pacific than elsewhere, in agreement with the observed reversal from heating to cooling. Observed brightness temperatures place the level at which cumulus anvils are most extensive very near the cold point over the equatorial Pacific. This, in turn, lies near the tropical tropopause throughout the Tropics. Collectively, these features suggest that the coldest cloud, found over the equatorial Pacific, plays a key role in maintaining temperature and humidity near the tropical tropopause.

1. Introduction

Humidity and thermal structure in the Tropics figure importantly in considerations of climate, transport of pollutants into the stratosphere, and the photochemistry of ozone. Each of these considerations is linked to the tropical tropopause. Despite its long-recognized importance, how the tropical tropopause is controlled remains under debate. Influencing it are several competing mechanisms which regulate thermal and humidity structure at upper levels. Closely related is the water budget of the stratosphere. It is forced by transport, associated with air ascending across the tropical tropopause.

Although its definition is not unique, the tropopause characterizes a transition from convective control of vertical structure to radiative control overhead. This tran-

Corresponding author address: Dr. Fabrizio Sassi, Atmospheric Systems and Analysis, 12995 Sheridan Blvd., Broomfield, CO 80020. E-mail: sassi@asac.org

sition is reflected in changes of tropopause temperature and height. With the outbreak of deep convection, the local tropopause ascends and assumes a colder temperature (Johnson and Kriete 1982; see also Tsuda et al. 1994). After the collapse of deep convection, the tropopause descends and assumes a warmer temperature. The coldest tropopause, in fact, is found at sites of a penetrative cloud, which has a temperature even colder than the analyzed tropopause (Gettelman et al. 2002). On seasonal timescales, tropopause heights and temperatures change by as much as 1 km and 10 K, respectively (Reid and Gage 1996). The tropopause is highest and coldest during northern winter, when the Australian monsoon positions deep convection near the equator.

This seasonality underscores another mechanism that influences the tropical tropopause. Northern winter is also when mean upwelling in the tropical stratosphere is strongest, driven then by amplified planetary waves of the Northern Hemisphere (Yulaeva et al. 1994). At 50 mb and above, the signature of mean upwelling is observed uniformly across the Tropics, consistent with the wave-driven circulation of the stratosphere. At lower levels, however, thermal structure is punctuated by strong zonal asymmetry that marks the localized influence of convection (Highwood and Hoskins 1998; Gettelman et al. 2002).

Closely related is the distribution of humidity. It plays a key role in the radiative energetics of the troposphere and lower stratosphere. By regulating total hydrogen, the humidity of tropospheric air entering the stratosphere also influences ozone photochemistry. Water vapor is transported upward inside convection, wherein condensation and the release of latent heat warm the Tropics. At 200 mb and below, humidity is positively correlated with cold clouds (Soden and Fu 1995; Sassi et al. 2001). Convection thus acts to warm and humidify the upper troposphere. This contrasts, however, with thermal structure and humidity at higher levels. Near the tropical tropopause, conditions are anomalously cold and dry. In fact, the coldest and driest conditions are found over the equatorial Pacific, coincident with deep convection (Atticks and Robinson 1983). The reversal of humidity structure between the upper troposphere and lower stratosphere is central to understanding whether air crossing the tropical tropopause acts to humidify the stratosphere or to dehydrate it.

Issues surrounding humidity are complicated by uncertainties over its distribution in the upper troposphere and lowermost stratosphere. Mixing ratio decreases there to only a few ppmv, challenging the sensitivity of operational radiosondes. Conventional measurements are also hampered by nonuniform coverage, which leaves vast regions over the oceans unobserved. Measurements by the operational satellites, on the other hand, are limited by coarse vertical resolution, which provides few independent levels. They are also restricted to clear-sky regions, wherein IR radiances are not saturated.

This study integrates measurements from several sources to explore how the tropical tropopause and surrounding conditions are maintained. Measurements of water vapor come from the Microwave Limb Sounder (MLS) on board the *Upper Atmospheric Research Satellite* (*UARS*). The microwave technique of MLS provides humidity in cloudy as well as clear-sky regions. Those observations have been mapped synoptically, providing a daily record of global humidity structure. They are complemented here by observations of cold clouds in high-resolution global cloud imagery (GCI), which have been composited from multiple satellites simultaneously observing the earth. Available globally every 3 h, the GCI provides a continuous record of convection, against which we compare humidity structure from MLS and contemporaneous thermal and dynamical structure in the European Centre for Medium-Range Weather Forecasts (ECMWF) analyses. Following a description of the data, section 3 discusses the time-mean 3D distributions of cold clouds, humidity, and thermal structure. To elucidate how that structure is maintained, section 4 then calculates changes that operate coherently with changes of deep convection. The observed behavior is interpreted in section 5 in terms of mechanisms controlling humidity and thermal structure.

2. Data

MLS is a limb-viewing instrument that relies on a passive microwave technique to observe atmospheric structure (Waters et al. 1999). It is distinguished from conventional satellite measurements by its ability to observe humidity in cloudy as well as clear-sky regions. Unlike nadir-viewing microwave measurements, MLS recovers humidity over continental regions as well as maritime regions. These features enable MLS to provide a uniform description of water vapor, with global coverage of the Tropics.

Measurements of water vapor are available from MLS via two separate retrievals: below 100 mb, relative humidity is retrieved via a tropospheric algorithm from radiances of the 205-GHz channel (Read et al. 1995). Data used here are from the version 4.9 retrieval (Read et al. 2001), which provides humidity at 464, 315, 215, and 146 mb. Separated by approximately 2.7 km, those levels represent tropospheric humidity where conventional measurements are inaccurate and with much finer vertical resolution than is available from nadir-viewing satellite measurements. At and above 100 mb, water vapor mixing ratio is retrieved via a stratospheric algorithm (Pumphrey 1999; Pumphrey et al. 2000). It recovers structure with vertical resolution comparable to that of the tropospheric retrieval. At 100 mb, however, the stratospheric retrieval is vulnerable to clouds, unlike the tropospheric retrieval at lower levels. Jointly, the two retrievals of microwave radiance provide continuous global coverage of tropical humidity from 300 mb upward.

Observations of water vapor recovered by these re-

trievals are asynoptic. They have been mapped synoptically via the method described by Salby and Sassi (2001). This method rejects undersampled variance that dominates asynoptic observations of convective structure. By doing so, it recovers synoptic behavior that operates coherently on large scales that are resolved in the asynoptic data. The mapping procedure yields a daily record of global synoptic structure that reflects the organization of convective properties. Gaps of a couple of days, introduced routinely by the *UARS* yaw maneuver, are bridged during the mapping procedure through low-frequency interpolation (Sassi and Salby 1998). Once transformed into synoptic behavior, humidity can be analyzed in the same fashion as other field properties.

The instantaneous distribution of cold clouds is represented in the GCI. Constructed from the imagery data of six satellites simultaneously observing the earth, the GCI provides synoptic images of 11-μm brightness temperature: every 3 h, with global coverage and horizontal resolution of 0.5° (Tanaka et al. 1991; Salby et al. 1991). Its high spatial and temporal resolution, with complete coverage of the earth, yields a continuous description of deep convection invading the upper troposphere and lowermost stratosphere.

Supporting these satellite observations are analyzed thermal and dynamical structures in ECMWF reanalyses. Available 4 times daily, they follow from data assimilation by a model with diabatic initialization, which treats divergent motion in the Tropics. The ECMWF analyses are not without their limitations. They suffer from a warm bias at the tropical tropopause, albeit less than is present in other analyses (Pawson and Fiorino 1999; Randel et al. 2000). Relative humidity (RH) evaluated from analyzed temperature therefore underestimates actual RH. While having this limitation, the ECMWF analyses provide a continuous record of 3D dynamical structure. They are employed in this study to investigate changes of temperature and motion that are contemporaneous with changes of humidity observed by MLS and cold cloud in the GCI.

3. Time-mean structure

Behavior averaged over time reflects a balance between sources and sinks that force humidity and thermal structure. We consider structure averaged over 1 November 1991–28 February 1992: first for zonal-mean behavior, which is coupled to the Hadley circulation, and then for individual convective centers that drive the Walker circulation.

a. Zonal-mean structure

In the zonal mean, temperature (not shown) decreases upward, achieving a minimum of 194 K over the equator near 100 mb. Figure 1 plots zonal-mean potential temperature, as a function of latitude and height. Isentropes are expanded vertically inside a deep layer centered near

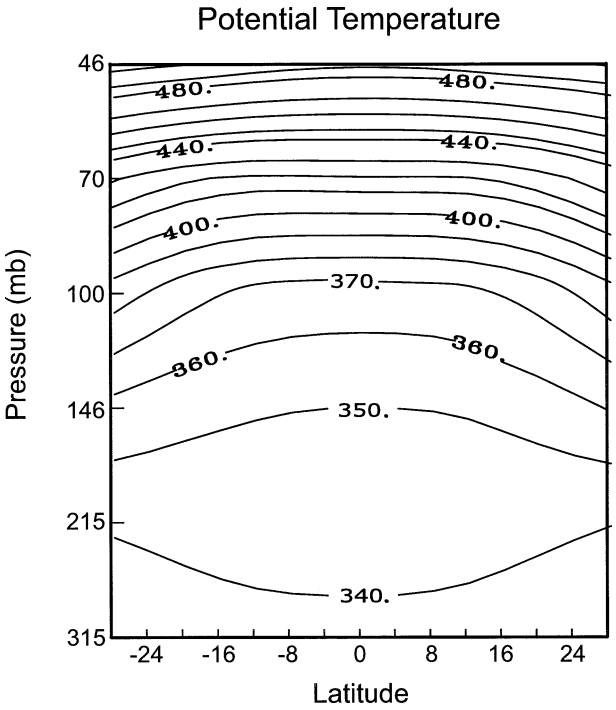

FIG. 1. Zonal-mean potential temperature, as a function of latitude and pressure during Nov 1991–Feb 1992.

$\theta = 345$ K, approximately 200 mb. Reduced stability ($\partial\theta/\partial z$) inside this layer reflects vertical mixing by convection. Convective mixing drives thermal structure toward a homogeneous distribution of equivalent potential temperature θ_e (approximately θ at these altitudes). Above $\theta = 370$ K, which passes through the cold point at 100 mb, stability increases sharply.

The structural change above and below $\theta \cong 345$ K reflects a reversal from heating to cooling: Below 345 K, isentropes are deflected downward, indicating heating of air in the Tropics. Above 345 K, they are deflected upward, indicating cooling of air in the Tropics. The reversal emerges clearly in the deviation of θ from its north–south average (Fig. 2). Below 345 K, anomalous θ is positive in the Tropics, implying heating relative to surrounding latitudes. Above 345 K, anomalous θ is negative in the Tropics, implying cooling. The implied cooling maximizes in a neighborhood of 100 mb. However, it is visible as high as 50 mb, where negative θ reflects an upward displacement of isentropes.

Figure 3 plots fractional cloud cover η (in percent), as a function of latitude and brightness temperature. Convection is deepest at 8°–4°S, where brightness temperatures are coldest. At brightness temperatures colder than 200 K (neighboring the tropopause), zonal-mean η has decreased to 1% and smaller. Nevertheless, brightness temperatures as cold as 185 K are found in the region of deepest convection. Note also that η decreases with height monotonically, from the midtroposphere upward into the lowermost stratosphere. Flanking the re-

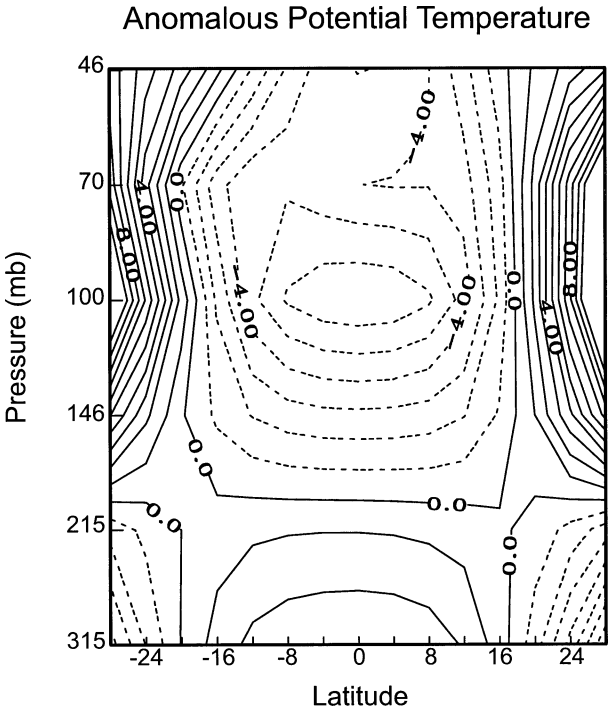

FIG. 2. As in Fig. 1, but for the deviation from the north–south mean.

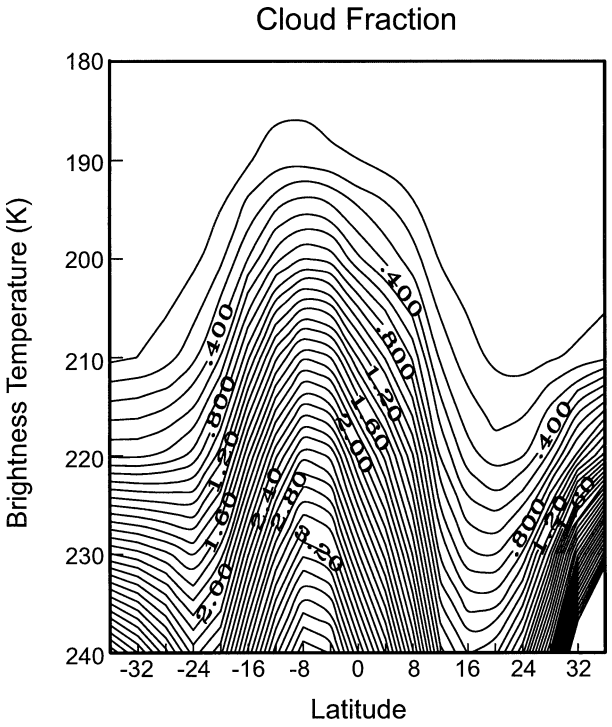

FIG. 3. Fractional coverage by cloud (in percent), as a function of latitude and brightness temperature during Nov 1991–Feb 1992.

gion of coldest cloud are latitudes in the subtropics of each hemisphere where deep convection is suppressed. They reflect subsidence in descending branches of the Hadley circulation.

The reversal of thermal structure near $\theta \cong 345$ K (Fig. 2) mirrors a similar reversal in the vertical autocorrelation of temperature, which is observed over the equatorial Pacific (Reid and Gage 1996). Implied are temperature changes of opposite sign about roughly the same level. Both features of vertical structure can be understood in terms of convection and its ventilation of upper levels with air from lower levels (e.g., Sherwood and Dessler 2001; Sassi et al. 2001). Convection is accompanied by detrainment of clouds and the subsequent mixing with its surroundings. Being irreversible, this process exerts a strong influence on cumulus clouds, as well as their environment.

Laboratory experiments show that a cumulus updraft behaves as a vortex ring; see Scorer (1978) for a review. Radial shear from the velocity maximum in the core of the updraft leads to entrainment of the surrounding air. Compensating such entrainment is detrainment of updraft air. This differential motion causes a section of updraft to turn itself inside out after advancing upward only 1–2 diameters. Air inside the updraft has then been diluted substantially with environmental air. Simultaneously, the environment has been ventilated with air from inside the updraft, which originated at lower levels. This exchange is irreversible. It drives environmental conditions toward those of air transported upward inside convection, tending to homogenize the vertical distribution of θ_e.

How a cumulus updraft influences thermal structure of the environment depends on its buoyancy (see, e.g., Salby 1996; Sherwood and Dessler 2001). An updraft's momentum is reinforced by buoyancy beneath its equilibrium level, or level of neutral buoyancy (LNB). At those levels, air inside the updraft is positively buoyant and hence warmer than its environment. Detrainment and mixing with the surroundings then act to warm the cloud's environment. The same process occurs above the LNB. However, the updraft's momentum is then opposed by buoyancy. Above the LNB, air inside the updraft is negatively buoyant and hence colder than its environment. Detrainment and mixing with the surroundings then act to cool the cloud's environment.

To leading order, the LNB corresponds to that level where environmental θ equals the θ_e of surface air, $\theta_e(0)$. Plotted in Fig. 4a is the surface distribution of time-mean θ_e plus one standard deviation: $\langle\theta_e\rangle(0)$. Derived from the record of ECMWF analyses, $\langle\theta_e\rangle(0)$ accounts for daily excursions of moist static energy. The $\langle\theta_e\rangle(0)$ maximizes in the Tropics, where values range between 350 and 370 K. Maximum moist static energy is found over the equatorial central Pacific.[1] Values of $\langle\theta_e\rangle(0)$ in the central Pacific approach 370 K. This is almost as

[1] The period under consideration coincided with a warm phase of El Niño-Southern Oscillation (ENSO), wherein convection and warm SST are displaced eastward from the western Pacific.

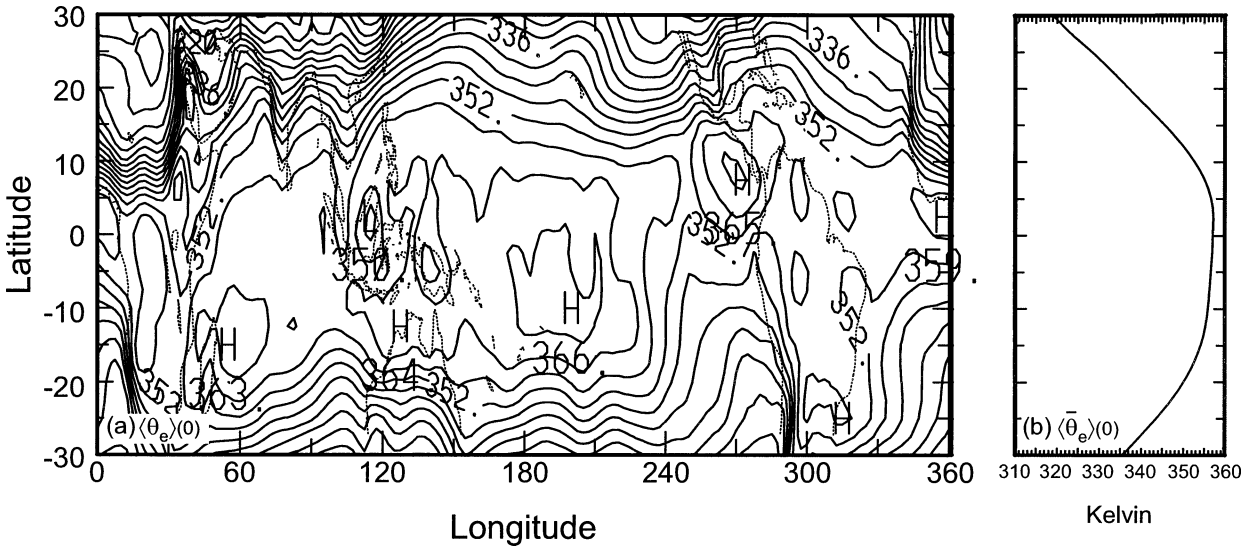

FIG. 4. (a) Geographical distribution of equivalent potential temperature at the surface plus one std dev, $\langle\theta_e\rangle(0)$, in K. (b) Corresponding zonal-mean distribution as a function of latitude.

high as the cold point, through which passes the $\theta =$ 370-K isentrope (Fig. 1). It lies at the top of the layer of weak stability. This is significantly higher than the reversal of thermal structure in Figs. 1 and 2, where implied heating changes sign. In the zonal mean (Fig. 4b), $\langle\theta_e\rangle(0)$ is somewhat lower but still well above the observed reversal from implied heating to cooling.

This picture is modified importantly by entrainment of surrounding air. By diluting the buoyancy of a cumulus updraft, entrainment siphons off moist static energy. Convection therefore reaches a level of neutral buoyancy with lower θ_e than it would under conservative conditions. Figure 5a plots the corresponding distribution of θ_e at the LNB: $\langle\theta_e\rangle$(LNB), inclusive of entrainment. It has been calculated for individual sites from local environmental conditions and the differential equation governing a cumulus updraft in the presence of entrainment, following the development in Salby (1996). The pattern of $\langle\theta_e\rangle$(LNB) resembles that of $\langle\theta_e\rangle(0)$ (Fig. 4a), to which it reduces under conservative conditions. However, values in the Tropics are reduced significantly. The value of $\langle\theta_e\rangle$ (LNB) varies between 340 and 350 K. In the zonal mean (Fig. 5b), $\langle\bar{\theta}_e\rangle$(LNB) $\cong$ 346 K. This is close to the observed reversal from heating to cooling in Figs. 1 and 2. The highest values are still found over the central Pacific, where $\langle\theta_e\rangle$(LNB) reaches 350 K. This places the LNB in that region near 150 mb (Fig. 1), some 3 km higher than the zonal mean.

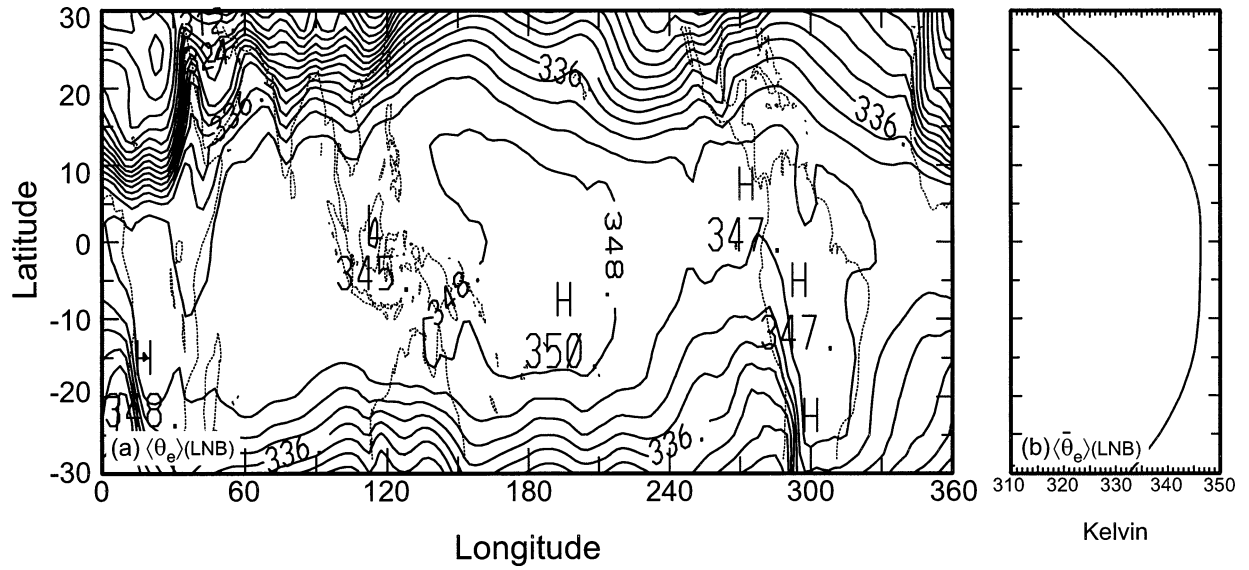

FIG. 5. As in Fig. 4, but at LNB, accounting for entrainment of cumulus updrafts (see text).

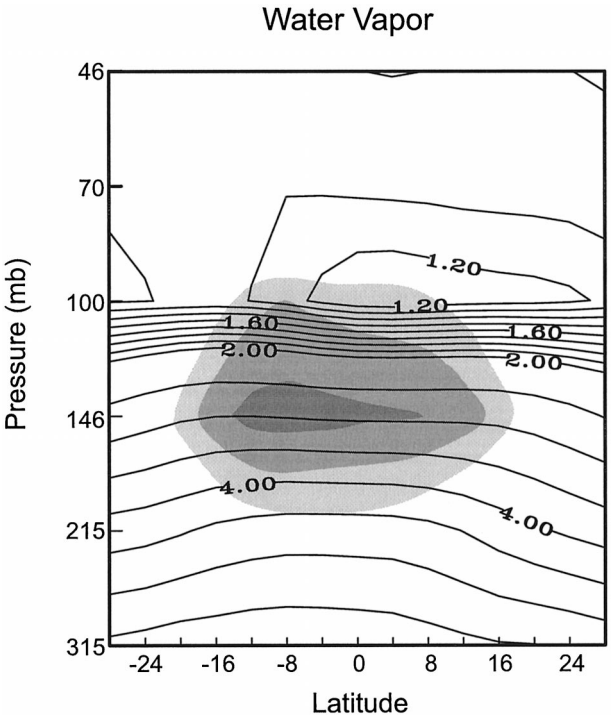

FIG. 6. Logarithm of zonal-mean mixing ratio, as a function of latitude and pressure, during Nov 1991–Feb 1992. Shaded is RH greater than 60%, 70%, and 80%.

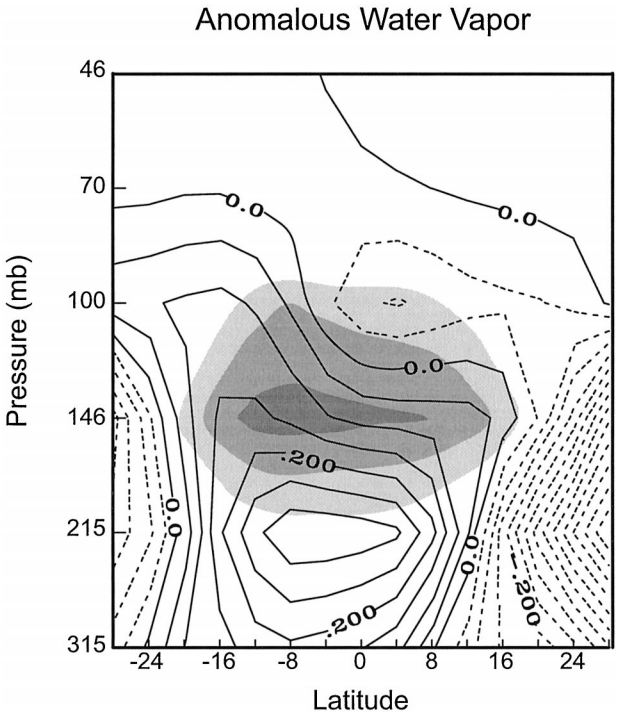

FIG. 7. As in Fig. 6, but for the deviation from the north–south mean. Shaded is RH greater than 60%, 70%, and 80%.

A cumulus updraft is warmer than its environment below the LNB, but colder than it above the LNB. Cumulus detrainment thus represents a heat source for the environment below $\theta \cong 345$ K, but a heat sink at higher levels. The fractional area covered by this mechanical source of heating and cooling is small, only a couple of percent in the zonal mean (Fig. 3). However, air advected horizontally through convective centers and mixing with their outflow can affect the entire Tropics in a matter of days.

The same process forces the humidity structure. Figure 6 plots the logarithm of mass mixing ratio r (contoured), as a function of latitude and height. Humidity increases equatorward, maximizing at 8°–4°S. These latitudes coincide with deep convection and the coldest cloud (Fig. 3). Zonal-mean r decreases upward, attaining a minimum of 3.0 ppmv at 100 mb. A higher levels, r varies with altitude slowly compared to the exponential variation seen below.

The distinct minimum of r near 100 mb extends northward into the winter hemisphere. Analogous structure is visible in seasonal-mean behavior observed by the Halogen Occultation Experiment (HALOE; Jackson et al. 1998; Randel et al. 2001). According to Figs. 6 and 3, deep convection marks the southern edge of the driest air near the tropopause: the dry anomaly emerges from those latitudes where r at lower levels is enhanced, which in turn coincides with the coldest cloud. After emerging from the region of deepest convection, dry air extends northward across the equator and into the winter hemisphere.

Superposed in Fig. 6 is zonal-mean relative humidity (shaded). As cloud fraction at these levels is only a couple of percent (Fig. 3), RH nearly equals environmental relative humidity (i.e., outside the cloud). RH increases upward. It exceeds 80% in a neighborhood of 150 mb, maximizing at latitudes of deep convection. The pattern of RH is qualitatively similar to one calculated in a chemical transport model from observed motion (Gettelman et al. 2000). Notice that the zone of nearly saturated environmental conditions is found just beneath the driest air. It divides levels at which humidity structure is reversed: below ~125 mb, contours of r are deflected upward, representing enhanced humidity in the Tropics. Conversely, above ~125 mb, contours of r are deflected downward, representing reduced humidity in the Tropics. Similar structure is apparent in seasonal-mean humidity observed by HALOE (Jackson et al. 1998).

The reversal of humidity structure near 125 mb emerges clearly in the deviation from the north–south average (Fig. 7). Anomalous mixing ratio is positive in the Tropics, reflecting humidification relative to surrounding latitudes. It maximizes at 8°–4°S between 300 and 150 mb, coincident with the cold cloud (Fig. 3). Enhanced r inside this region reflects cumulus detrainment, which humidifies the environment as the cloud mixes with its surroundings and dissolves (Soden and Fu 1995; Sassi et al. 2001). Capping the region of en-

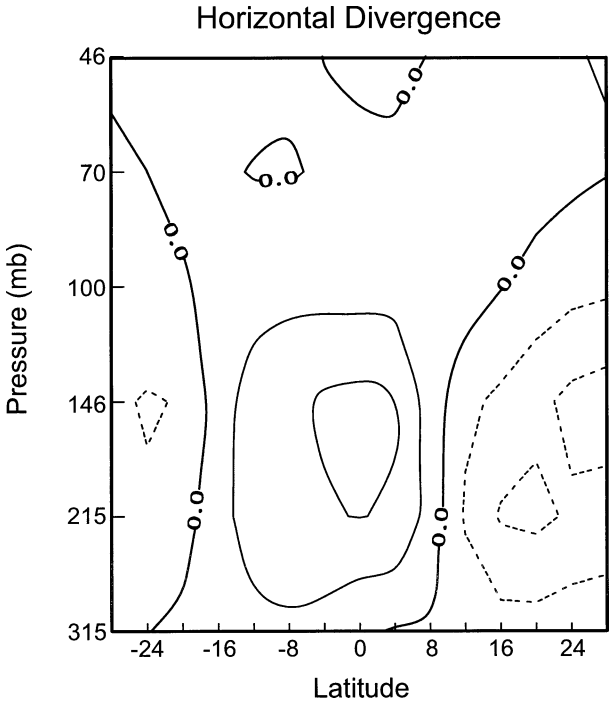

FIG. 8. Zonal-mean horizontal divergence, as a function of latitude and pressure during Nov 1991–Feb 1992.

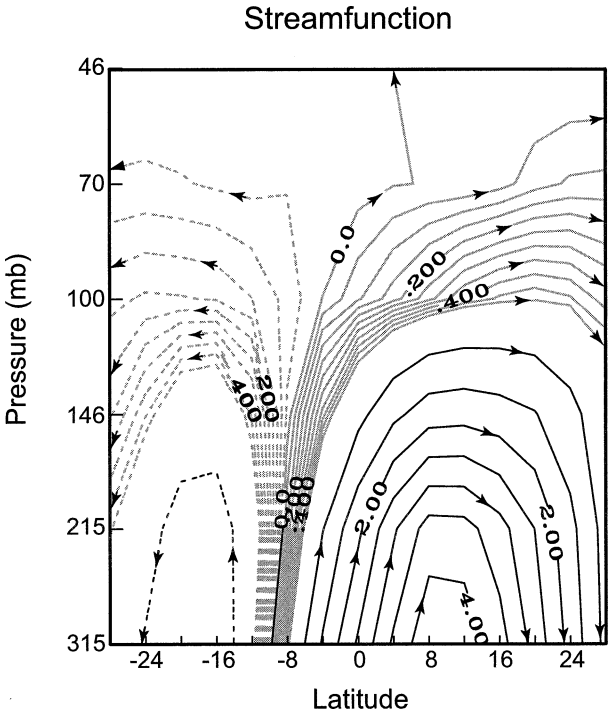

FIG. 9. Zonal-mean streamfunction, as a function of latitude and pressure during Nov 1991–Feb 1992. Note reduced contour increment for values within ±0.50 of zero.

hanced r is the maximum of RH. The horizontal structure of RH mirrors that of anomalous r, which is likewise coincident with the cold cloud.

Immediately above the maximum of RH, anomalous mixing ratio reverses sign: anomalous r becomes negative above ~125 mb. There, it reflects dehydration relative to surrounding latitudes. From the coldest cloud at 8°–4°S, anomalously dry air extends northward, joining even drier air at lower levels of the winter hemisphere.

Latent heating inside convection drives upwelling, which diverges in the upper troposphere. Figure 8 plots zonal-mean horizontal divergence, $\nabla \cdot \mathbf{v}$, as a function of latitude and height. Horizontal divergence is positive from 300 mb upward. Maximizing at and south of the equator, it reflects convective outflow that is associated with detraining cumulus anvils. The pattern of divergence is consistent with the horizontal distribution of the cold cloud (Fig. 3), as well as with the anomalous mixing ratio (Fig. 7). Notice, however, that positive $\nabla \cdot \mathbf{v}$ extends to levels higher than anomalous r. Whereas $\nabla \cdot \mathbf{v}$ remains positive up to almost 70 mb, anomalous r decreases above 200 mb—at and above levels where RH exceeds 60%.

Flanking positive divergence is negative $\nabla \cdot \mathbf{v}$ in the subtropics of each hemisphere. There, convective outflow converges to form subsidence. Strongest in the winter hemisphere, it coincides with reversals of anomalous r toward drier conditions outside the Tropics (Fig. 7). It also coincides with the suppression of the cold cloud, visible at the same latitudes (Fig. 3). Notice that $\nabla \cdot \mathbf{v}$ reverses sign near 70 mb. At those levels, air converges weakly over the equator, just above the coldest cloud (Fig. 3).

The calculation of $\nabla \cdot \mathbf{v}$ determines the zonal-mean streamfunction $\overline{\psi}$ through continuity and requiring motion to vanish far overhead. Plotted in Fig. 9, $\overline{\psi}$ describes the zonal-mean Hadley circulation: upwelling is strong at and south of the equator, inside the region of deep convection (Fig. 3). Above 200 mb, it veers poleward, chiefly into the winter hemisphere. There, it becomes a strong northward motion that maximizes at 200–150 mb. (Note the change of contour increment above ~100 mb.) Northward motion, however, is visible as high as 50 mb. At these levels, it composes the equator-to-pole branch of the Brewer–Dobson circulation (e.g., Dunkerton 1989). Notice that, above 100 mb, time-mean streamlines are deflected upward—in both hemispheres. Relative to time-mean isentropes (Fig. 1), they describe $\dot{\theta} > 0$ and diabatic upwelling.

Comparison with Fig. 7 indicates that, in the zonal mean, air rises inside the region of deep convection. Below 125 mb, this motion acts to humidify the environment. After passing through the zone of nearly saturated environmental conditions (RH > 80%), air inside the region of deep convection continues to rise. However, at those levels, it acts to dehydrate the environment. The source of dehydrated air is marked by the minimum of r in Figs. 6 and 7. It emerges from latitudes

of the coldest cloud, above the zone of nearly saturated environmental conditions. Anomalously dry air then extends northward along streamlines into the winter hemisphere; see also Randel et al. (2001).

The reversal of humidity structure near 125 mb, like that of the thermal structure in Fig. 2, can be understood in terms of convection and its ventilation of upper levels with air from lower levels. Beneath the zone of nearly saturated environmental conditions, air inside a cumulus updraft has a total water loading (vapor plus cloud ice) that exceeds its surroundings. Detrainment and subsequent mixing with drier environmental air dilutes the total water loading of cloudy air, leading to sublimation and cloud dissolution. As it dissolves the cloud, this process humidifies the environment, consistent with the anomalously moist air found below 125 mb (Fig. 7).

At levels of nearly saturated environmental conditions, the foregoing process is modified importantly. Cloud dissolution is then inhibited because environmental air is not much drier than the cloud into which it is mixed. Environmental air is, therefore, less effective at dissolving clouds that detrain from a cumulus updraft.[2] Reduced sublimation at levels of high RH favors increased cloud ice, greater opportunity for particles inside the updraft to coalesce into large ones, and hence greater opportunity for their removal through precipitation. This process is analogous to the dehydration mechanism for an anvil proposed by Danielsen (1982, 1993); see also Sherwood and Dessler (2001). However, it has implications for air continuing upward inside a cumulus updraft.

After passing through the zone of nearly saturated environmental conditions, an updraft would be depleted of total water. The same effect would be realized if large particles, lofted overhead, fall rapidly back to lower levels. Simultaneously, air inside the updraft would experience decreasing RH at higher levels. This restores unsaturated environmental conditions, favoring a return to cloud dissolution via mixing with drier surrounding air. However, with its total water loading depleted, a cumulus updraft ascending above the RH maximum would be anomalously dry. Upon mixing with its surroundings, that cloudy air would therefore dehydrate environmental air. This interpretation is consistent with the anomalously dry air found above 125 mb (Fig. 7). Environmental air that has been dehydrated in this fashion would then extend from the minimum of r atop convection, northward along streamlines (Fig. 9).

The cooling and dehydration found above convection may also involve radiative considerations. Radiative cooling, however, requires the presence of ice at stratospheric levels (Johnson and Kriete 1982). Thin cirrus can form at those levels through adiabatic cooling as air is deflected over the convective tower, for example, as in pileaus or cap clouds (Holton and Gettelman 2001). Radiative interaction with thick anvils below can then produce diabatic cooling (Hartmann et al. 2001). Gradual sedimentation of cirrus ice would act to dehydrate stratospheric air as it passes over a convective center. In this fashion, thin cirrus can augment the cooling and dehydration of the environment accomplished by cumulus detrainment. It is noteworthy, however, that the reversal from heating to cooling is found very near the LNB (Figs. 2, 5b). This relationship holds separately inside individual convective centers, as will be seen below.

b. Structure inside convection

Cold cloud fraction is actually concentrated longitudinally, inside centers of convection. Figure 10 plots the horizontal distribution of η in the upper troposphere and, separately, at the tropical tropopause. At brightness temperatures of 240–230 K (Fig. 10a), near 250 mb, cloud fraction approaches 10% from Africa across the Indian Ocean, over the central Pacific, and again over South America. Contrasting with this extensive structure is η at temperatures of 200–190 K (Fig. 10b), near 100 mb. Neighboring the tropical tropopause, cloud fraction at this level is dominated by the contribution from the central Pacific. There, η is 2–3 times greater than it is over the Indian Ocean and South America. The change of structure reflects the horizontal distribution of $\langle\theta_e\rangle$(LNB) in Fig. 5. It describes an LNB that is highest over the central Pacific, some 3 km higher than elsewhere.

As in all convective centers, η at these levels is contributed chiefly by a stratiform cloud that accompanies the cumulus tower, which will be treated synonymously with the anvil. Figure 11 plots, as a function of brightness temperature, fractional coverage by anvil η_A (solid), defined from the GCI as an aggregate of contiguous cold pixels. Superposed is the fractional coverage by tower and turret η_T (dashed), defined as isolated cold pixels. Over the central Pacific (Fig. 11a), η_A is almost an order of magnitude greater than η_T throughout much of the upper troposphere. It extends vertically through a deep layer, reaching brightness temperatures colder than 185 K. However, at temperatures colder than 210 K (near 150 mb), η_A decreases sharply from a plateau found at warmer temperature.[3] The decrease of cloud fraction is found at about the same level as the LNB over the central Pacific.

Over South America (Fig. 11b), vertical profiles of η_A and η_T are distinctly shallower. Both cloud categories are limited to temperatures warmer than 200 K. Now η_A decreases sharply at brightness temperatures colder

[2] The horizontal extent of the cumulus anvil exhibits a conspicuous maximum at these levels (see Fig. 12), reflecting greater longevity as the anvil diverges away from its moisture supply inside the cumulus updraft.

[3] The sharp decrease at these temperatures is even more conspicuous in the histogram of raw 8-km radiances, from which the 50-km GCI pixels are produced (see Sassi et al. 2001, their Fig. 2).

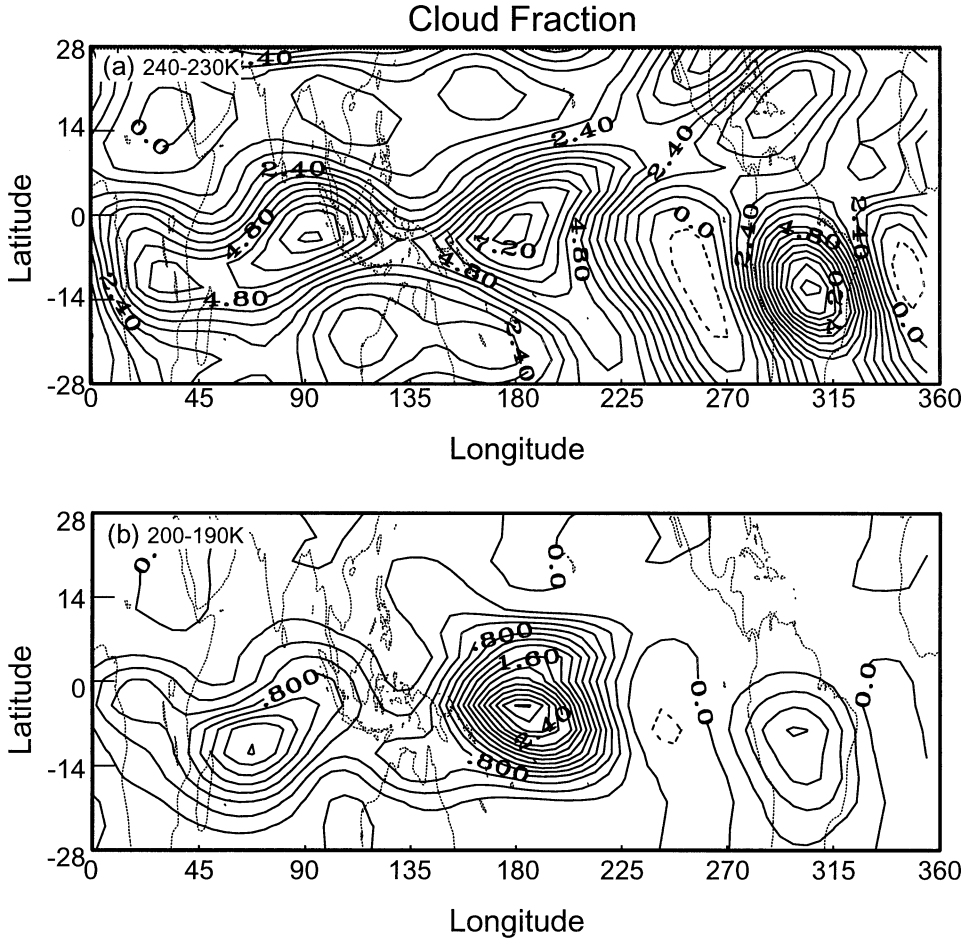

FIG. 10. Fractional coverage (in percent) by cloud at brightness temperatures of (a) 240–230 K near 250 mb, and (b) 200–190 K near 100 mb.

than 230 K (near 250 mb). As over the central Pacific, the decrease of cloud fraction is found at about the same level as the LNB over this site. Notice that, over South America, the anvil in the upper troposphere occupies nearly twice the area that it does over the central Pacific. However, at temperatures colder than 210 K, η_A over the central Pacific dominates through the deeper penetration of clouds.

The change of cloud structure at upper levels is also evident in the mean areal extent of individual anvils (Fig. 12). Although total cloud fraction decreases with height monotonically (Fig. 11), the mean areal extent of the anvils increases. This may reflect the deeper penetration of larger convective systems, which better isolate the updraft. Over the central Pacific (Fig. 12a), the extent of individual anvils increases conspicuously at brightness temperatures of 220–190 K. This is about the level at which η_A decreases sharply, which in turn coincides with the LNB. Implied is a sharp reduction of updraft, compensated by a widening of surrounding anvils. A maximum is reached at 200 K (150–100 mb), where the mean areal extent of individual anvils is greatest.

Owing to the finite optical depth of anvils, actual cloud top lies even higher than is indicated in Fig. 12a. Lidar measurements provide enhanced sensitivity to cloud particles. They indicate that the top of cirrus anvils can reside as much as a kilometer higher than is indicated by narrowband IR radiances, like those used to produce the GCI (Heymsfield et al. 1991). Accounting for this limitation of satellite measurements places the peak of η_A near 190 K. This is about 2 K colder than the tropopause at this site, some 4 K colder than the zonal mean.

Over South America (Fig. 12b), the extent of individual anvils also reaches a maximum. However, it is found at 220–210 K, nearly 3 km lower. As over the central Pacific, this coincides with the sharp decrease of η_A (Fig. 11), which in turn neighbors the LNB over South America. In contrast, the maximum extent of the anvils lies distinctly lower than the tropopause over South America. As elsewhere in the Tropics, the tro-

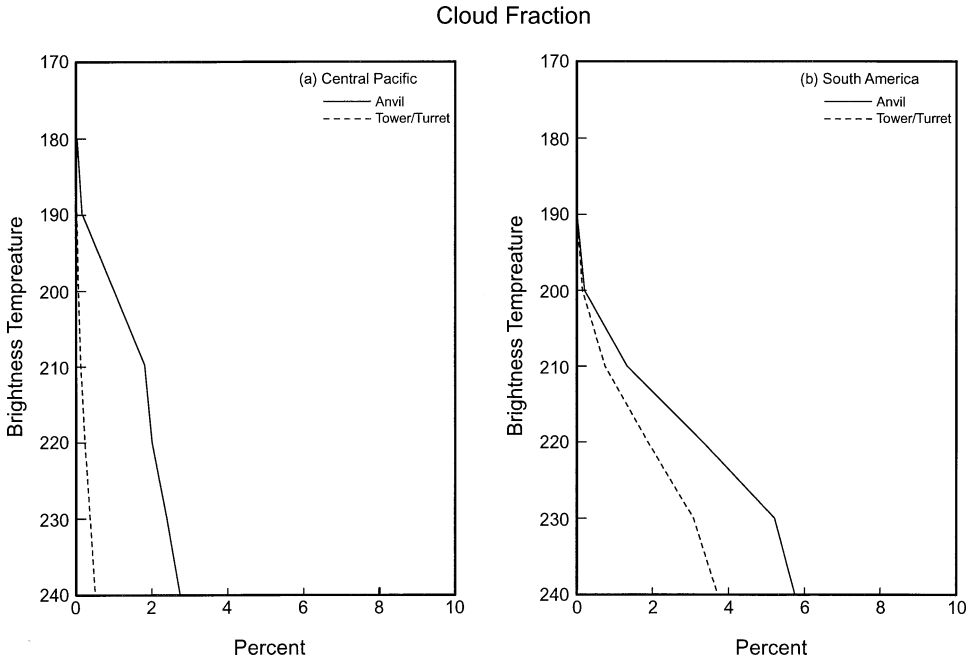

FIG. 11. Fractional coverage by anvil η_A (solid), defined as contiguous cold pixels, and by tower and turret η_T (dashed), defined as isolated cold pixels, as a function of brightness temperature, for (a) the central Pacific and (b) South America.

popause is found near 100 mb—close to the level over the central Pacific where the extent of anvils is greatest.

Notice that, at brightness temperatures of 220 K and warmer, the mean areal extent of anvils over South America is actually 50%–100% greater than that over the central Pacific. Consistent with total η at those brightness temperatures (Fig. 10), this distinction may stem from the diurnal nature of convection over South America. Diurnal heating generates anvils simultaneously across the convective center, enabling cloud from neighboring convective systems to coalesce.

Cloud structure in Figs. 11 and 12 is in broad agreement with extinction measurements from the Cryogenic Limb Array Etalon Spectrometer (CLAES), which characterize ice particles (Read et al. 2001). Those measurements saturate near 150 mb, reflecting maximum loading by cloud ice. Both features of cloud structure coincide with the zone of nearly saturated environmental conditions (Fig. 6). They are consistent with reduced sublimation and increased longevity of the anvil, as it detrains from cumulus updrafts.

The differences of cold clouds in Fig. 12 reflect differences of thermal structure between the convective centers. Over South America, the cold point has a temperature of ~194 K, close to the zonal-mean value. The same is true over the Indian Ocean. Over the central Pacific, however, the coldest cloud is more abundant. There, the cold point has decreased to 192 K, a couple of Kelvin colder than the zonal mean. The central Pacific is also where the cumulus cloud overshoots the local tropopause, a feature that coincides with the coldest tropopause (Gettelman et al. 2002). In contrast, cumulus clouds at other sites seldom reach the tropopause, which resides at about the same elevation. The association suggests a relationship between the coldest cloud, found over the central Pacific, and the tropopause throughout the Tropics.

In each convective center, the anomalous thermal structure (not shown) resembles that of the zonal mean (Fig. 2). It reflects warming in the Tropics below a level near $\theta \cong 345$ K and cooling above. However, over the central Pacific, the reversal from implied heating to cooling is found near 350 K, some 3 km higher than over South America. Isentropes over the central Pacific are expanded vertically more than elsewhere in the Tropics. Accompanying this feature is the greatest reduction of static stability, which changes out of phase with tropopause height (Johnson and Kriete 1982; Seidel et al. 2001). Both features of thermal structure are found over that region where the cold cloud is most abundant (Fig. 10b).

The central Pacific is also distinguished by humidity structure. Mixing ratio there achieves its smallest values, approaching 2.9 ppmv. This is somewhat greater than the 2.2 ppmv reported locally in HALOE observations (Jackson et al. 1998).[4] However, both values retrieved

[4] The synoptic mapping procedure through which MLS data have been processed here retains only the six gravest zonal wavenumbers. Variance at higher wavenumbers is undersampled in the asynoptic measurements. The synoptic structure thus represents behavior that is averaged over large scales, those which have been properly sampled.

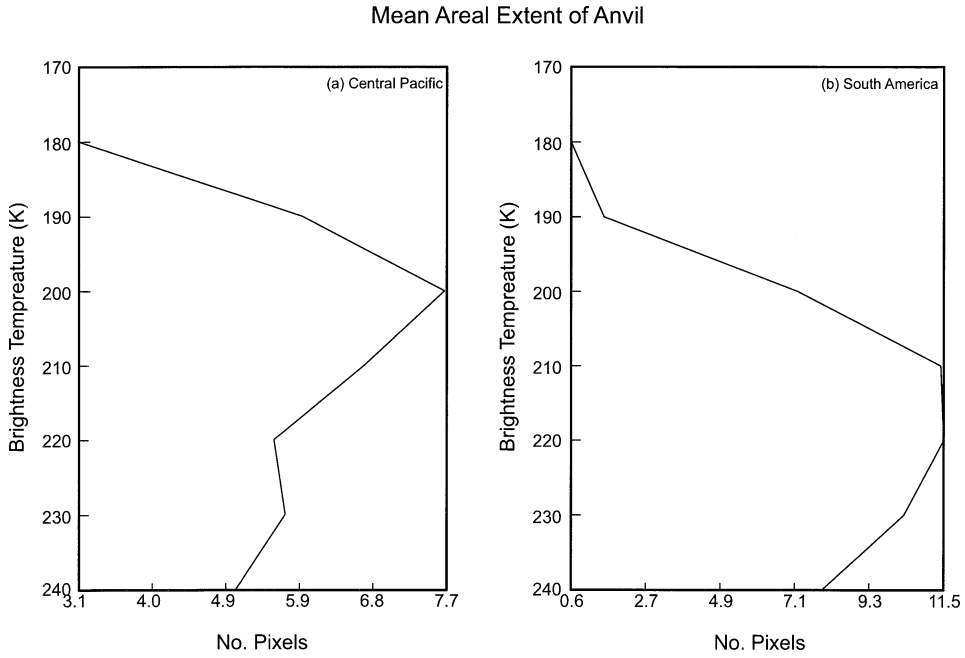

FIG. 12. Mean areal extent of anvils (in number of 0.5° pixels), as a function of brightness temperature, for (a) the central Pacific and (b) South America.

by satellite are substantially greater than the 0.7 ppmv sounded locally in the neighborhood of individual convective towers (Vömel et al. 1995). The substantial difference reflects the limb-viewing geometry of MLS and HALOE, which averages humidity over about 200 km. Time averaging has a similar impact.

Figure 13 plots the anomalous mixing ratio (departure from the north–south mean). Over the central Pacific

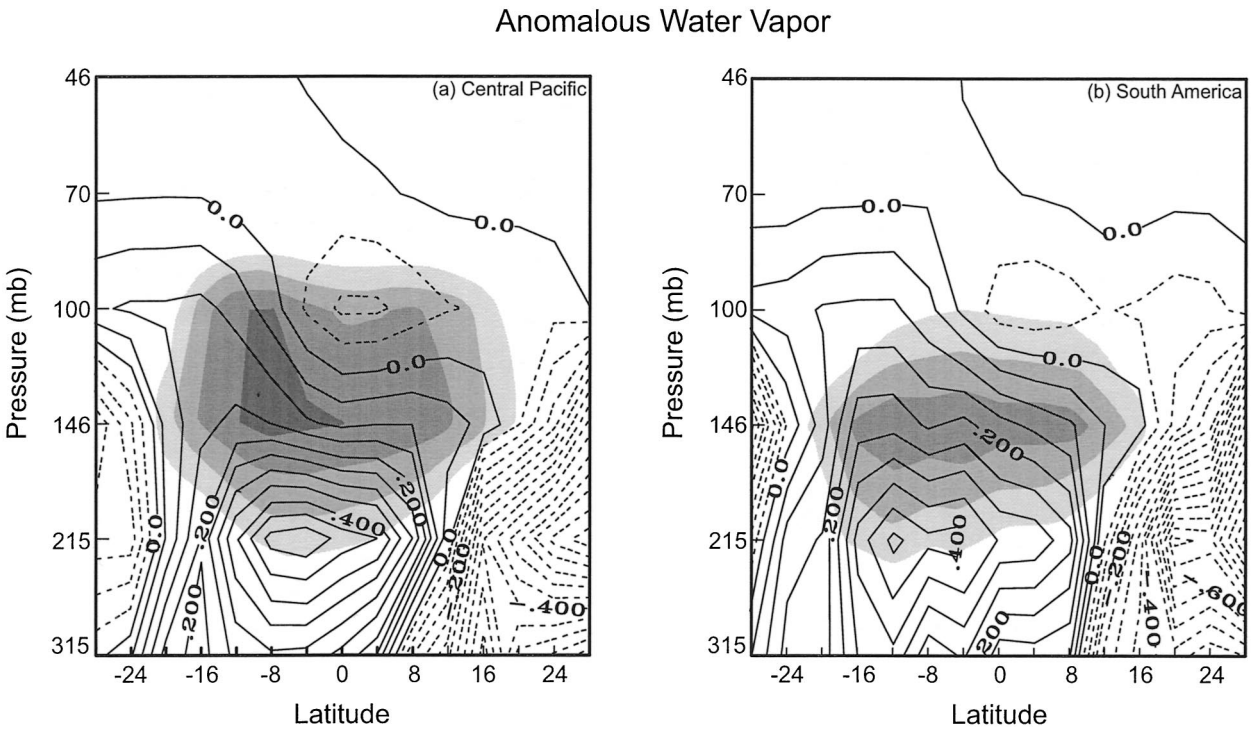

FIG. 13. As in Fig. 7, but over (a) the central Pacific and (b) South America.

(Fig. 13a), anomalous r becomes negative above 125 mb. Anomalously dry air appears above a deep layer of nearly saturated environmental conditions (shaded). Here RH exceeds 80% from 150 to 100 mb. It exceeds 90% where the layer is deepest, near 8°S, coincident with the coldest cloud (Fig. 3). In fact, RH actually reaches 95% inside this zone. In light of the warm bias of ECMWF analyses, conditions inside this zone are virtually saturated, if not supersaturated. They characterize environmental air that is almost cloudy. Coinciding with the zone of nearly saturated environmental conditions is the greatest areal extent of individual anvils (Fig. 12a).

Over South America (Fig. 13b), anomalous mixing ratio reverses at about the same level. At this site, however, r only decreases to 3.2 ppmv. About the same value is observed over the Indian Ocean (not shown). At both sites, environmental RH exceeds 80% only within a shallow layer near 150 mb. It does not reach 90%. Accompanying the reduced RH in the uppermost troposphere is smaller η over South America at brightness temperatures colder than 200 K (Fig. 10b).

Notice that, whereas RH is greater over the central Pacific, r at these levels is smaller than over South America. Enhanced RH over the central Pacific thus follows, not from humidification, but from cooling, which sharply reduces the saturation mixing ratio. Also noteworthy is the base of nearly saturated environmental conditions. Even though the LNB and cloud fraction differ between the convective centers, the level at which environmental conditions approach saturation does not. In fact, RH exceeds 80% above 150 mb across much of the Tropics. This feature of saturated conditions suggests the involvement of a universal mechanism, one that is invariant between convective centers.

Above the zone of nearly saturated environmental conditions, anomalous r over each convective center reverses sign. Anomalously dry air extends northward into the winter hemisphere, where it joins drier air at lower levels. The negative anomaly weakens above 70 mb, eventually yielding to a uniform structure. However, the signature of convection is clearly visible to at least 70 mb ($\theta = 430$ K); see also Clark et al. (2001). This observation is in accord with balloon measurements over the equatorial Pacific, which reveals evidence of convective mixing as high at 19 km (Vömel et al. 1995), and with overshooting cumulus, which occasionally extend as high as 20 km (Simpson et al. 1998). For the zonal asymmetries in Fig. 13 to be maintained, they must be continually resupplied with dessicated air.

The limited occurrence of clouds at these levels has been argued as making convection incapable of explaining the low humidity characteristic of the tropical tropopause. Chemical measurements imply comparatively weak transport of surface air above 14 km (Folkins et al. 1999). However, calculations with similar measurements point to the importance of cumulus detrainment, which dehydrates the upper levels (Dessler 2002). Over the central Pacific, deep cumulus penetrates well above 14 km to brightness temperatures colder than 185 K (even colder when the optical depth is accounted for). Tropospheric air supplied to those levels by overshooting cumulus is then extremely cold and dry—much colder and drier than environmental conditions (see also Pfister et al. 1993; Vömel et al. 1995). Through detrainment and subsequent mixing, such clouds serve as a mechanical heat sink and moisture sink for the environment. Environmental conditions are then driven toward the extremely cold temperature and dry humidity of air that has been processed inside the convection.

Also distinguishing the central Pacific is horizontal divergence, which represents convective outflow. Horizontal divergence is compared in Fig. 14 between the central Pacific and South America. Over the central Pacific (Fig. 14a), $\nabla \cdot \mathbf{v}$ extends upward across a deep layer, from 300 to almost 70 mb. Mirroring the deep vertical structure of η (Fig. 11a), it reflects convective outflow and detrainment that ventilate the upper troposphere, tropopause, and the lowermost stratosphere with air from lower levels. Over the Indian Ocean (not shown), $\nabla \cdot \mathbf{v}$ has analogous structure. However, it achieves only 70% of the strength. More importantly, it does not penetrate above 100 mb. Over South America (Fig. 14b), $\nabla \cdot \mathbf{v}$ is only half as strong as over the central Pacific. It too is confined to a shallower layer, barely penetrating above 150 mb. As for RH, the difference of $\nabla \cdot \mathbf{v}$ between these sites parallels the marked difference in cold cloud fraction (Fig. 10b).

Above the divergence of each convective center is a region of weak convergence. Over the central Pacific, $\nabla \cdot \mathbf{v}$ becomes negative at 70–50 mb, just above the coldest cloud (Fig. 11a). Over South America, $\nabla \cdot \mathbf{v}$ becomes negative near 100 mb—distinctly lower, but again just above the coldest cloud (Fig. 11b). In tandem with horizontal divergence at lower levels, the horizontal convergence at stratospheric levels implies downwelling that prevails immediately beneath it. Below the region of convergence, stratospheric air descends into the uppermost troposphere, where it joins and then diverges with the major outflow from convection. This interpretation is consistent with stratospheric downwelling that has been reported over the equatorial Pacific (Gage et al. 1991; Sherwood 2000). It is also consistent with anomalous motion found here to operate coherently with the outbreak of deep convection, as will be seen shortly.

4. Changes operating coherently with convection

We now consider how the fields discussed above vary in relation to deep convection. The life cycle of an individual field property χ is composited against horizontal divergence in the upper troposphere. Serving as a reference time series, $\overline{\nabla \cdot \mathbf{v}}$ is averaged over those latitudes and pressures where horizontal divergence is large (Figs. 8, 14). The composite structure and evolution then follow from the cross covariance between χ

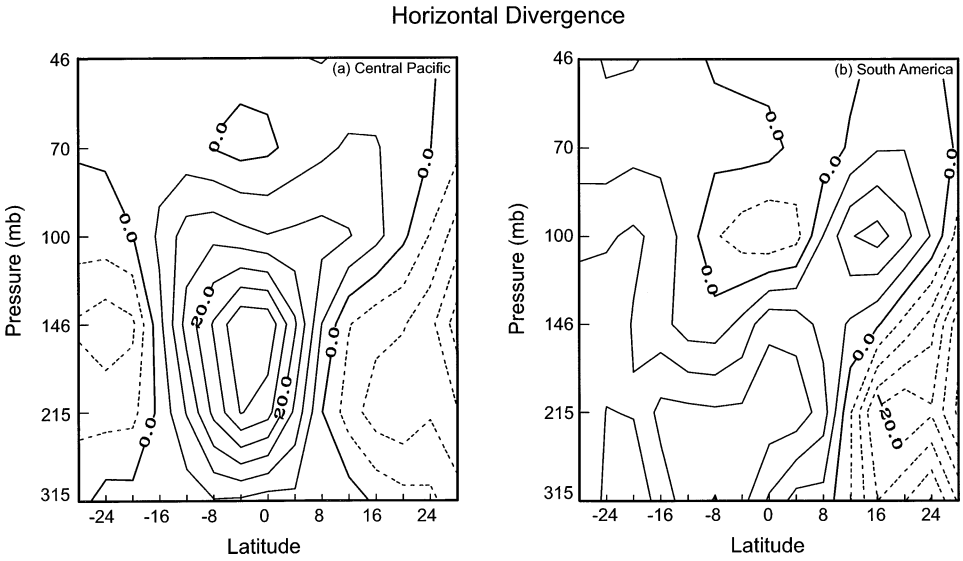

FIG. 14. As in Fig. 8, but over (a) the central Pacific and (b) South America.

and $\overline{\nabla \cdot \mathbf{v}}$, renormalized by their respective variances (see, e.g., Hendon and Salby 1994). If $c[\chi, \overline{\nabla \cdot \mathbf{v}}](\mathbf{x}, \tau)$ is the correlation, for lag τ, between the field variable χ at location $\mathbf{x}$ and the reference time series $\overline{\nabla \cdot \mathbf{v}}$, then the composite life cycle of χ reduces to

$$\hat{\chi}(\mathbf{x}, \tau) = c[\chi, \overline{\nabla \cdot \mathbf{v}}](\mathbf{x}, \tau) \cdot \langle \chi^2 \rangle^{1/2}(\mathbf{x}). \quad (1)$$

Here $\hat{\chi}(\mathbf{x}, \tau)$ describes the anomalous structure of the field property that operates coherently with changes of tropical outflow from deep convection.

We concentrate on changes in relation to zonal-mean divergence (Fig. 8), which represents the collective outflow of convection that compose the Hadley circulation. Field properties composited against the divergence over individual convective centers behave similarly to those deduced earlier from the time-mean structure.

Zonal-mean behavior

Figure 15 plots the horizontal distribution of cold clouds operating coherently with zonal-mean divergence: at lags of $\tau = -8$, 0, and $+8$ days. Regions where their covariance is significant at the 95% and 99% levels are shaded. At lag -8 days (Fig. 15a), preceding maximum outflow in the upper troposphere, anomalous η is positive and strong over the Indian Ocean. It reflects an enhancement of cold clouds. A weaker positive anomaly appears over the western Pacific. Both positive anomalies are compensated for over the date line by negative anomalous η, where the cold cloud is suppressed. It reflects anomalous downwelling of the Walker circulation.

At lag 0 (Fig. 15b), contemporaneous with maximum outflow in the upper troposphere, the cold cloud is sharply enhanced south of the equator. Anomalous η represents an outbreak of deep convection over the Indian Ocean and western Pacific. The cold cloud is also enhanced over South America. Simultaneously, η is suppressed across a wide zone of longitude immediately north of the equator. There, negative η reflects anomalous downwelling of the Hadley circulation.

At lag $+8$ days (Fig. 15c) following maximum outflow, η has decreased—mostly over the Indian Ocean. This leaves the positive anomaly over the western Pacific to dominate. The eastward shift of positive anomalous η between $\tau = -8$ and $+8$ days is reminiscent of the seesaw pattern over the Indian Ocean and western Pacific as the Madden–Julian Oscillation (MJO) propagates across those regions (Weickman and Khalsa 1990; Zhu and Wang 1993; Salby and Hendon 1994). In fact, a signature of the MJO is registered during this period in upper-tropospheric humidity (Sandor et al. 1998; Mote et al. 2000; Sassi et al. 2002).

Figure 16 plots anomalous θ operating coherently with zonal-mean divergence, at lag 0, when both are strong. Represented in isobaric coordinates, anomalous θ has the same structure as anomalous temperature, T. Changes of thermal structure are strongly coherent with convective outflow (shaded)—in the troposphere as well as in the lower stratosphere. This stage of the life cycle corresponds to the outbreak of deep convection (Fig. 15b). Anomalous θ is then weakly positive across much of the tropical troposphere. There, it reflects anomalous heating below the LNB and a downward displacement of isentropes.

The behavior is consistent with cumulus detrainment, which warms the environment below the LNB and drives it toward a uniform distribution of θ. As the characteristic time between convective episodes is only a matter of days, thermal structure never deviates far from this limiting state. The adjustment during convection is, therefore, weak. Stronger positive θ appears in

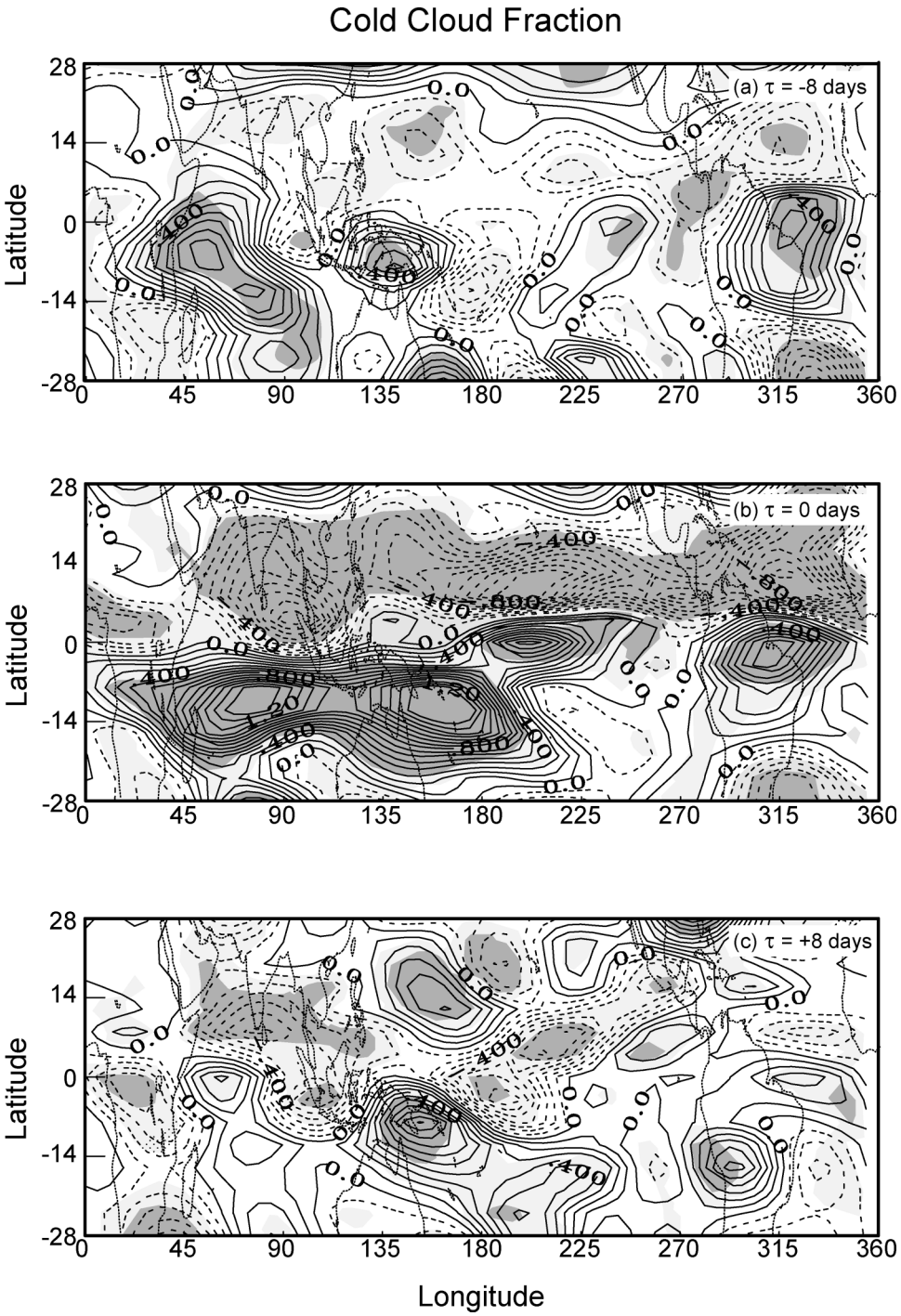

FIG. 15. Variation of cloud fraction at 150 mb operating coherently with zonal-mean convective outflow (see text) at lags of (a) −8, (b) 0, and (c) +8 days. Shading marks significance greater than 95% (lighter) and 99% (darker).

the subtropics, where it reflects adiabatic warming and downwelling that compensates for upwelling inside the region of convection (cf. Fig. 3).

Above 150 mb, anomalous θ reverses sign. Strong negative values there coincide with the sharp vertical gradient of time-mean θ (Fig. 1). They reflect anomalous cooling above the LNB and an upward displacement of isentropes. Together with the downward displacement at lower levels, this change expands the vertical separation of isentropes above and below 150 mb. In terms

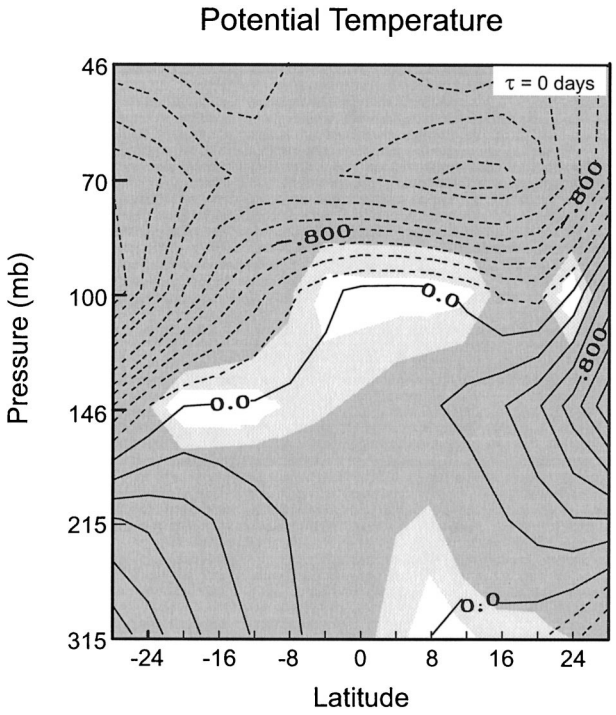

FIG. 16. Change of zonal-mean potential temperature, at lag 0, operating coherently with zonal-mean convective outflow. Shading marks significance greater than 95% (lighter) and 99% (darker).

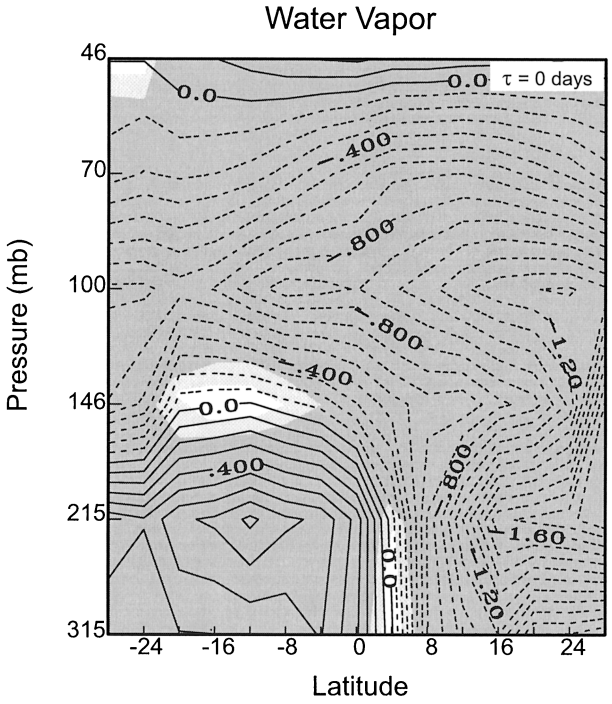

FIG. 17. As in Fig. 16, but for the logarithm of the mixing ratio.

of temperature, the change above 150 mb represents an upward extension of a strong positive lapse rate during the outbreak of deep convection. The behavior is analogous to changes of tropopause temperature and height observed by radiosondes (Johnson and Kriete 1982). Implied is a reduction of static stability which, in turn, varies out of phase with tropopause elevation. The change of stability is magnified at upper levels, where a weak or negative lapse rate that develops radiatively is replaced by a strong positive lapse rate that is forced by convection. Anomalous structure of $N^2 = (g/\theta)(\partial\theta/\partial z)$ (not shown), in fact, reveals a weakening of stability that maximizes near 100 mb, but extends upward of 70 mb.

Figure 17 plots anomalous mixing ratio, also at lag 0. Like thermal structure, changes of humidity are strongly coherent with tropospheric outflow (shaded)—in the troposphere as well as in the lower stratosphere. Within the troposphere, anomalous r is positive at latitudes of convection, representing humidification of the environment. The positive anomaly is consistent with cumulus detrainment of moist air. As for time-mean r, the positive anomaly is limited to levels beneath a zone of nearly saturated environmental conditions at this stage (not shown); it resembles the zone of high RH in time-mean structure (Fig. 7). At higher levels, anomalous r reverses sign, There, negative anomalous r reflects dehydration of the environment. It can be understood in terms of cumulus detrainment of dessicated air that has passed through the zone of nearly saturated environmental conditions. The negative anomaly maximizes near 100 mb, but is visible almost to 50 mb. From latitudes of deepest convection (Fig. 15b), it extends northward into the winter hemisphere.

Plotted in Fig. 18 is the anomalous streamfunction, also at lag 0. The anomolous streamfunction reflects an intensification of the Hadley circulation. Accompanying the amplification of convection is anomalous northward motion through 100 mb, which becomes downwelling at subtropical latitudes of the winter hemisphere. Notice that the latter coincides with the suppression of the cold cloud at lag 0 (Fig. 15b). At latitudes of deep convection, anomalous streamlines extend upward as high as 70 mb. On the summer side of convection, they continue upward to the highest level. On the winter side, anomalous streamlines reaching 70 mb veer horizontally, coincident with the dry anomaly (Fig. 17), and then descend into the winter hemisphere.

A region of stratospheric downwelling prevails from 8°S northward. It lies at and just beneath the region of zonal-mean convergence (Fig. 8). The latter, in turn, resembles convergence over the central Pacific (Fig. 14a), which resides atop the coldest cloud (Fig. 11a). In Fig. 18, northward and descending motion at stratospheric levels is reinforced by a reversed cell just overhead. The reversed cell acts to draw air equatorward from the winter hemisphere, where conditions are warmer and moister. Between the anomalous Hadley cell and the reversed cell overhead, anomalous streamlines converge—inside the region of convergence near 70 mb

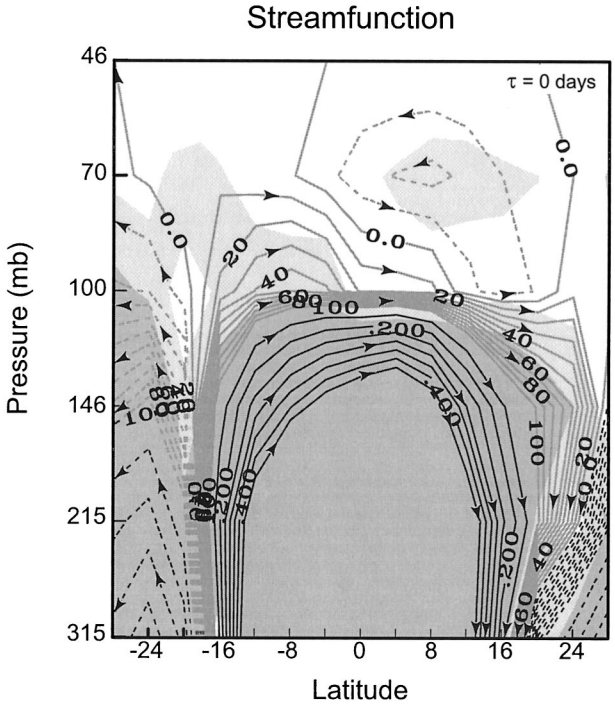

FIG. 18. As in Fig. 16, but for zonal-mean streamfunction. Note reduced contour increment for values within ±0.50 of zero (scaled by 1000).

that is situated atop the coldest cloud. Temperature at and below this region is noteworthy (Fig. 16). Anomalous downwelling is accompanied, not by increased temperature, which would reflect adiabatic warming, but by reduced temperature, that reflects diabatic cooling. The source of diabatic cooling is presumably also responsible for the upward extension of the lapse rate and the anomalously cold temperature that accompany the outbreak of deep convection (Johnson and Kriete 1982).

Collectively, these features imply that the outbreak of deep convection is attended by diabatic cooling and dehydration of the environment, at and just above the tropopause. A radiative mechanism for such cooling was considered earlier by Johnson and Kriete (1982) and references therein. However, as recognized there, radiative cooling requires the presence of ice above the tropopause. Subvisible cirrus has been observed at stratospheric levels. Radiative cooling inside such clouds can drive downwelling, like that found over deep convection. In addition, the growth and eventual sedimentation of cirrus ice particles would act to dehydrate stratospheric air passing over a convective center.

Microphysical calculations confirm the feasibility of this dehydration mechanism (Jensen et al. 2001). However, they indicate that it would leave air substantially supersaturated, with environmental RH of 110%–160%. This is well above observed values, although perhaps not when the warm bias of ECMWF analyses is accounted for. More fundamental, however, is the ice loading at stratospheric levels. Even if sufficient ice is present, radiative adjustment at the very cold temperatures neighboring the tropical tropopause operates on a timescale longer than a month. This is much longer than the observed timescale of anomalous temperature, humidity, and stratospheric motion. They all amplify on the timescale of convection, on the order of a day in ECMWF analyses. In radiosonde observations, the cold anomaly above convection amplifies on a timescale that is even shorter, on the order of hours (see Johnson and Kriete 1982). As noted by those authors, the region of cooling assumes nearly adiabatic vertical structure. Accompanying it in the lower troposphere is warming, which operates on the same timescale. Implied is reduced stability, which in turn varies out of phase with tropopause elevation.

Figure 19 presents, for 150 mb, the horizontal distribution of anomalous r (contoured) and motion, both at lag 0. As before, regions coherent at the 95% and 99% levels are shaded. Divergence from the centers of convection in Fig. 15b is marked by a strong southeasterly flow from the equatorial Indian Ocean and central Pacific. This contrasts with only weak motion over South America, where divergence is confined to lower levels (Fig. 14). Negative anomalous r extends from the equator, northward across the subtropics of the Eastern Hemisphere. It reflects environmental air that has been dehydrated. That dry air emerged, earlier during the life cycle, from the two convective centers along its southern edge. From convection over the Indian Ocean and central Pacific, negative anomalous r extends northward and westward along anomalous streamlines. It eventually joins midlatitude westerlies, which carry dehydrated air eastward. The dry anomaly that emerges from the equatorial Indian Ocean and central Pacific is strongly coherent with divergence in the upper troposphere. Repeated outbreaks of deep convection then favor anomalously dry conditions over the same range of longitudes in time-mean structure, as was observed by HALOE (Randel et al. 2001).

In addition to horizontal transport, r in the winter hemisphere is also influenced by vertical transport. At 150 mb, the anomalous zonal-mean streamfunction (Fig. 18) places downwelling at latitudes north of 4°N. The anomalous circulation therefore transports drier air downward from the minimum of r near 100 mb (Fig. 6). This introduces negative anomalous r across much of the winter subtropics, where cold cloud is suppressed (Fig. 15b). Analogous structure is visible in wintertime-mean humidity from HALOE (Jackson et al. 1998).

5. Conclusions

Thermal and humidity structures near the tropical tropopause operate coherently with the cold cloud that invades upper levels. So does anomalous vertical motion associated with the Hadley and Walker circulations. Examined during November 1991–February 1992, these

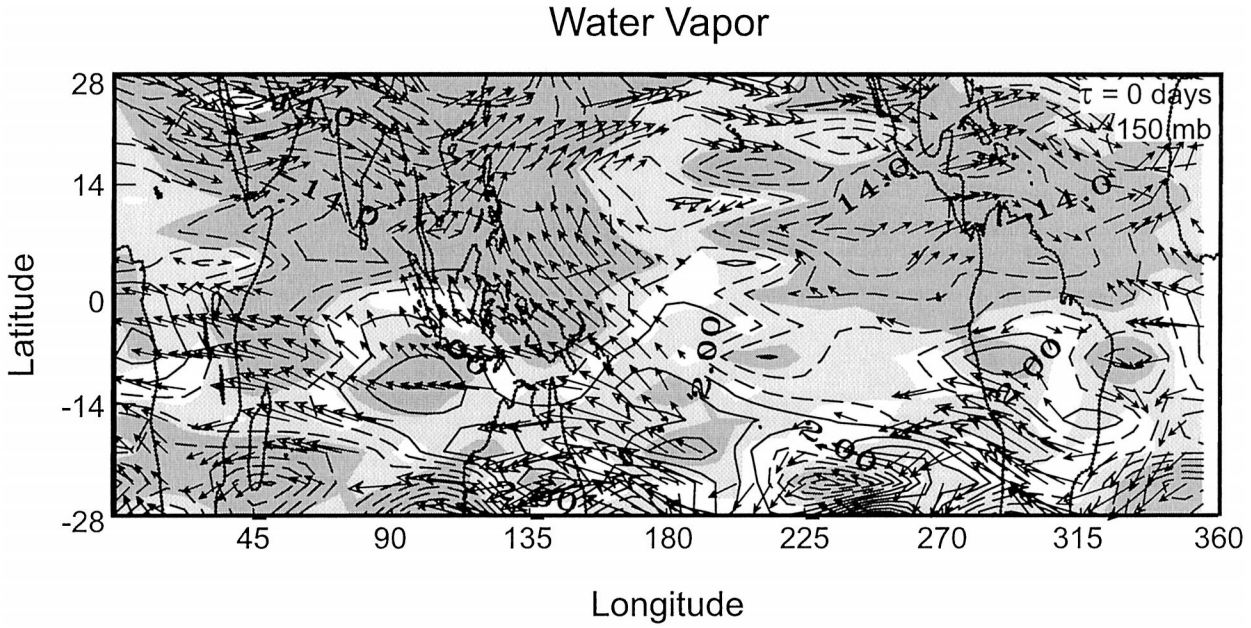

FIG. 19. Geographical distribution of mixing ratio (contoured) and horizontal motion (vectors), at lag 0, operating coherently with zonal-mean convective outflow. Shading marks significance greater than 95% (lighter) and 99% (darker).

fields all vary coherently with the outflow from convective centers—in the troposphere as well as in the lowermost stratosphere.

The outbreak of deep convection is accompanied by diabatic heating below a level between 250 and 150 mb, but by diabatic cooling at higher levels. Coinciding with diabatic cooling are stratospheric convergence and downwelling. Anomalous stratospheric motion amplifies simultaneously with divergence at tropospheric levels, which characterizes the major outflow from deep convection. The appearance of coherent changes in these field properties points to deep convection as playing a central role in controlling thermal structure near the tropical tropopause.

Anomalous thermal structure is broadly consistent with cumulus detrainment. Through irreversible mixing, that process serves as a heat source for the environment below the LNB, but as a heat sink at higher levels. Calculations, inclusive of entrainment, place the LNB very near the observed reversal from heating to cooling, consistent with this interpretation. Cumulus detrainment serves as a mechanical source of heating and cooling, one that operates on the same timescale as convection. At stratospheric levels, that mechanism may be augmented by radiative cooling inside subvisible cirrus. It too accompanies deep convection, influencing thermal structure at similar levels but on a longer timescale. Associated with the outbreak of convection, these processes account for much of the variance of thermal structure near the tropical tropopause. The residual (i.e., variance that operates incoherently with convection) may stem from changes of mean upwelling in the tropical stratosphere, associated with the wave-driven circulation.

A similar interpretation applies to water vapor. The outbreak of deep convection is accompanied by humidification below 125 mb, but by dehydration at higher levels. The reversal from humidification to dehydration can likewise be understood in terms of cumulus detrainment. Cloud dissolution and mixing with the environment serve as a source of water vapor below those levels where environmental conditions approach saturation. However, they serve as a sink of water vapor at higher levels, if cumulus updrafts have been dessicated after passing through the zone of nearly saturated environmental conditions. The same effect results if large particles that are lofted overhead fall rapidly back to lower levels. This interpretation is supported by the mean areal extent of cirrus anvils, as well as extinction measurements of cloud ice. Both maximize at the same levels as RH. Dehydration of the environment through cumulus detrainment may be augmented by sedimentation of cirrus ice, which operates at similar levels.

The deepest convection is found over the central Pacific, or to its west during the cold phase of ENSO. This site coincides with the highest moist static energy. The latter yields an LNB that is some 3 km higher over the equatorial Pacific than elsewhere. Agreeing with this feature is the observed reversal from heating at lower levels to cooling overhead: it changes between sites in similar fashion, being some 3 km higher over the equatorial Pacific. The behavior is consistent with cumulus detrainment and its dependence on the LNB.

The equatorial Pacific is also where the tropopause

temperature is coldest, a couple of Kelvin colder than the zonal mean. This distinction mirrors the distribution of the very cold cloud. During the period considered, the cumulus clouds penetrates deeply over the equatorial Pacific, reaching several km higher than over other convective centers. When the optical depth of the cloud is accounted for, observed brightness temperatures place the level of most extensive anvil and cumulus detrainment very near the cold point over the equatorial Pacific. This, in turn, lies near the zonal-mean tropopause. The coincidence of these features suggests that cumulus detrainment over the equatorial Pacific, perhaps supported by subvisible cirrus, exerts a major influence on the tropopause throughout the Tropics.

Mirroring the distribution of clouds, as well, is horizontal divergence. It is positive through a deep layer over the equatorial Pacific, extending to almost 70 mb. This is also the site of driest air. Slightly drier than the zonal mean, dehydrated air over the equatorial Pacific appears just above a deep layer in which environmental conditions are nearly saturated. Inside that layer, RH likewise assumes its greatest values. They reflect environmental conditions that are close to saturation, if not supersaturated. Those conditions suggest the efficient removal of total water from cumulus updrafts, leaving dessicated air to ventilate the environment at higher levels.

Collectively, these features imply that the coldest cloud, found over the equatorial Pacific, serves as a major source of tropospheric air at and just above the tropopause. After being processed inside cumulus updrafts, such air is extremely cold and dry—far colder and drier than environmental conditions. By supplying such air, cold clouds over the equatorial Pacific can play a key role in maintaining temperature and humidity near the tropical tropopause.

Acknowledgments. The authors are grateful for constructive comments provided by a reviewer. This work was performed while the authors were supported by NASA Grant NAG5-6692 and NSF Grant ATM-0121853.

REFERENCES

Atticks, M. G., and G. D. Robinson, 1983: Some features of the structure of the tropical tropopause. *Quart. J. Roy. Meteor. Soc.,* **109,** 295–308.

Clark, H., A. Billingham, R. Harwood, and H. Pumphrey, 2001: Water vapor in the tropical lower stratosphere during the driest phase of the atmospheric tape recorder. *J. Geophys. Res.,* **106,** 22 695–22 705.

Danielsen, E. F., 1982: Dehydration mechanism for the stratosphere. *Geophys. Res. Lett.,* **9,** 605–608.

——, 1993: In situ evidence of rapid, vertical, irreversible transport of lower tropospheric air into the lower tropical stratosphere by convective cloud turrets and by larger-scale upwelling in tropical cyclones. *J. Geophys. Res.,* **98,** 8665–8681.

Dessler, A., 2002: The effect of deep tropical convection on the tropical tropopause layer. *J. Geophys. Res.,* **107,** 4033, doi: 10.1029/2001JD000511.

Dunkerton, T. J., 1989: Nonlinear Hadley circulation driven by asymmetric differential heating. *J. Atmos. Sci.,* **46,** 956–974.

Folkins, I., M. Loewenstein, J. Podolske, and M. Proffitt, 1999: A barrier to vertical mixing at 14 km in the Tropics: Evidence from ozonesondes and aircraft measurements. *J. Geophys. Res.,* **104,** 22 095–22 102.

Gage, K., J. McAfee, D. Carter, W. Ecklund, A. Riddle, G. Reid, and B. Balsley, 1991: Long-term vertical motion over the tropical Pacific: Wind profiling doppler radar measurements. *Science,* **254,** 1771–1773.

Gettelman, A., J. Holton, and A. Douglass, 2000: Simulations of water vapor in the lower stratosphere and upper troposphere. *J. Geophys. Res.,* **105,** 9003–9023.

——, M. L. Salby, and F. Sassi, 2002: Distribution and influence of convection in the tropical tropopause region. *J. Geophys. Res.,* **107,** 4080, doi:10.1029/2001JD001048.

Hartmann, D., J. Holton, and Q. Fu, 2001: The heat balance of the tropical tropopause, cirrus, and stratospheric dehydration. *Geophys. Res. Lett.,* **28,** 1969–1972.

Hendon, H. H., and M. L. Salby, 1994: The life cycle of the Madden–Julian Oscillation. *J. Atmos. Sci.,* **51,** 2225–2237.

Heymsfield, G., R. Fulton, and J. Spinhirne, 1991: Aircraft overflight measurements of midwest severe storms: Implications on geosynchronous satellite interpretations. *Mon. Wea. Rev.,* **119,** 436–456.

Highwood, E. J., and B. J. Hoskins, 1998: The tropical tropopause. *Quart. J. Roy. Meteor. Soc.,* **124,** 1579–1604.

Holton, J., and A. Gettelman, 2001: Horizontal transport and the dehydration of the stratosphere. *Geophys. Res. Lett.,* **28,** 2799–2802.

Jackson, D., S. Driscoll, E. Highwood, J. Harries, and J. Russell, 1998: Troposphere to stratosphere transport at low latitudes as studied using HALOE observations of water vapour 1992–1997. *Quart. J. Roy. Meteor. Soc.,* **124,** 169–192.

Jensen, E., L. Pfister, A. Ackerman, A. Tabazadeh, and O. Toon, 2001: A conceptual model of the dehydration of air due to freeze-drying by optically thin, laminar cirrus rising slowly across the tropical tropopause. *J. Geophys. Res.,* **106,** 17 237–17 252.

Johnson, R., and D. Kriete, 1982: Thermodynamic circulation characteristics of winter monsoon tropical mesoscale convection. *Mon. Wea. Rev.,* **110,** 1898–1911.

Mote, P. W., H. L. Clark, T. J. Dunkerton, R. S. Harwood, and H. C. Pumphrey, 2000: Intraseasonal variations of water vapor in the tropical upper troposphere and tropopause region. *J. Geophys. Res.,* **105,** 17 457–17 470.

Pawson, S., and M. Fiorino, 1999: A comparison of reanalyses in the tropical stratosphere. Part 3. Inclusion of the presatellite data era. *Climate Dyn.,* **15,** 241–250.

Pfister, L., and Coauthors, 1993: Gravity waves generated by a tropical cyclone during the STEP tropical field program: A case study. *J. Geophys. Res.,* **98,** 8611–8638.

Pumphrey, H., 1999: Validation of a new prototype water vapor retrieval for the UARS Microwave Limb Sounder. *J. Geophys. Res.,* **104,** 9399–9412.

——, H. Clark, and R. Harwood, 2000: Lower stratospheric water vapor as measured by UARS MLS. *Geophys. Res. Lett.,* **27,** 1691–1694.

Randel, W., J. Wu, and D. Gaffen, 2000: Interannual variability of the tropical tropopause derived from radiosonde data and NCEP reanalyses. *J. Geophys. Res.,* **105,** 15 509–15 523.

——, ——, A. Gettelman, J. Russell, J. Zawodny, and S. Oltmans, 2001: Seasonal variation of water vapor in the lower stratosphere observed in HALOE data. *J. Geophys. Res.,* **106,** 14 313–14 325.

Read, W. G., J. Waters, D. A. Flower, L. Froidevaux, R. F. Jarnot, D. L. Hartmann, R. S. Harwood, and R. B. Rood, 1995: Upper Tropospheric Water Vapor from UARS MLS. *Bull. Amer. Meteor. Soc.,* **76,** 2381–2389.

——, and Coauthors, 2001: UARS Microwave Limb Sounder upper tropospheric humidity measurement: Method and validation. *J. Geophys. Res.,* **106** (D23), 32 207–32 258.

Reid, G. C., and K. S. Gage, 1996: The tropical tropopause over the western Pacific: Wave driving, convection, and the annual cycle. *J. Geophys. Res.,* **101,** 21 233–21 241.

Salby, M., 1996: *Fundamentals of Atmospheric Physics.* Academic Press, 627 pp.

——, and H. H. Hendon, 1994: Intraseasonal behavior of clouds, temperature, and motion in the Tropics. *J. Atmos. Sci.,* **51,** 2220–2237.

——, and F. Sassi, 2001: Synoptic mapping of convective structure in undersampled satellite observations. *J. Climate,* **14,** 2281–2295.

——, H. H. Hendon, K. Woodberry, and K. Tanaka, 1991: Analysis of global cloud imagery from multiple satellites. *Bull. Amer. Meteor. Soc.,* **72,** 467–480.

Sandor, B., W. Read, J. Waters, and K. Rosenlof, 1998: Seasonal behavior of tropical to midlatitude upper-tropospheric water vapor from UARS MLS. *J. Geophys. Res.,* **103,** 25 935–25 947.

Sassi, F., and M. Salby, 1998: Fast Fourier Synoptic Mapping of UARS data. *J. Geophys. Res.,* **103,** 10 885–19 898.

——, ——, and W. G. Read, 2001: Relationship between upper tropospheric humidity and deep convection. *J. Geophys. Res.,* **106,** 17 133–17 146.

——, ——, H. C. Pumphrey, and W. G. Read, 2002: Influence of the Madden–Julian Oscillation on upper tropospheric humidity. *J. Geophys. Res.,* **107,** 4681, doi:10.1029/2001JD001331.

Scorer, R., 1978: *Environmental Aerodynamics.* Ellis Horwood Ltd., 487 pp.

Seidel, D. J., R. J. Ross, and J. K. Angell, 2001: Climatological characteristics of the tropical tropopause as revealed by radiosondes. *J. Geophys. Res.,* **106,** 7857–7878.

Sherwood, S., 2000: A stratospheric ''drain'' over the maritime continent. *Geophys. Res. Lett.,* **27,** 677–680.

——, and A. E. Dessler, 2001: A model for transport across the tropical tropopause. *J. Atmos. Sci.,* **58,** 765–779.

Simpson, J., J. Halverson, H. Pierce, C. Morales, and T. Iguchi, 1998: Eyeing the eye: Exciting early stage science results from TRMM. *Bull. Amer. Meteor. Soc.,* **79,** 1711.

Soden, B. J., and R. Fu, 1995: A satellite analysis of deep convection, upper-tropospheric humidity, and the greenhouse effect. *J. Climate,* **8,** 2333–2351.

Tanaka, K. H., K. Woodberry, H. H. Hendon, and M. L. Salby, 1991: Assimilation of global cloud imagery from multiple satellites. *J. Atmos. Oceanic Technol.,* **8,** 613–626.

Tsuda, T., Y. Murayama, H. Wiryosumarto, S. Woto, B. Harijono, and S. Kato, 1994: Radiosonde observations of equatorial atmosphere dynamics over Indonesia. 1. Equatorial waves and diurnal tides. *J. Geophys. Res.,* **99,** 10 491–10 505.

Vömel, H., S. Oltman, D. Kley, and P. Crutzen, 1995: New evidence for the stratospheric dehydration mechanism in the equatorial Pacific. *Geophys. Res. Lett.,* **22,** 3235–3238.

Waters, J. W., and Coauthors, 1999: The UARS and EOS Microwave Limb Sounder (MLS) experiments. *J. Atmos. Sci.,* **56,** 194–218.

Weickmann, K. M., and S. J. S. Khalsa, 1990: The shift of convection from the Indian Ocean to the western Pacific Ocean during a 30–60 day oscillation. *Mon. Wea. Rev.,* **118,** 964–978.

Yulaeva, E., J. R. Holton, and J. M. Wallace, 1994: On the cause of the annual cycle in tropical lower-stratospheric temperatures. *J. Atmos. Sci.,* **51,** 169–174.

Zhu, B., and B. Wang, 1993: The 30–60-day convection seesaw between the Indian and western Pacific Oceans. *J. Atmos. Sci.,* **50,** 184–199.